

Nonstationary deconvolution as applied to the Blackfoot broadband survey

Alana R. Schoepp and Gary F. Margrave

ABSTRACT

Nonstationary deconvolution (NSD) is designed to approximately correct seismic data for source signature and anelastic attenuation. The amplitude spectrum of the forward operator is designed by calculating the time-variant amplitude spectrum of the input data and then smoothing it to remove reflectivity. The amplitude spectrum of the operator can be combined with a minimum-phase spectrum, estimated with the Hilbert transform of the natural logarithm of the amplitude spectrum. The forward operator is then inverted and applied to the input data with nonstationary filter techniques. NSD is a data-driven method and can be thought of as a combination of stationary deconvolution and inverse-Q filtering.

NSD has been developed in two different modes. The NSD operator can be designed and applied for each individual trace (trace-by-trace NSD), or a single operator can be designed from the ensemble and applied to each trace (profile-mode NSD). The advantage to profile-mode NSD is that it has greater statistical leverage because it uses many traces to design one operator. This can lead to improved lateral stability of reflectivity estimates in noisy data.

Nonstationary deconvolution was applied to the Blackfoot broadband survey and the results were compared to the results from combinations of gain and Wiener deconvolution, and Wiener deconvolution and inverse-Q filtering. The NSD result displayed relative enhanced vertical resolution and improved reflectivity character. In addition, it delineated the target, an incised channel, more clearly than the other methods.

INTRODUCTION

The ultimate goal of seismic data processing is to recover the reflection coefficients of the subsurface. Part of the processing involved in achieving this end is removing the source signature and correcting for anelastic attenuation. A method is desired that will restore the diminished amplitudes, correct for the phase rotation and compensate for the attenuated frequencies. Two methods commonly used to treat this problem are a combination of gain and stationary deconvolution, and a combination of stationary deconvolution and inverse-Q filtering. A third method of correcting for these problems has been developed and is called nonstationary deconvolution (NSD).

This paper will begin with a brief overview of stationary deconvolution and inverse-Q filtering. Next, the methodology of NSD will be developed, starting with the spectral model upon which NSD is based. Finally, examples comparing the relative performance of these three techniques will be shown.

CONCEPTUAL OVERVIEW OF THE ALGORITHMS

Stationary deconvolution can approximately correct seismic data for source signature and frequency attenuation, however, it is not an ideal approach because it does not take the time-variant manner of attenuation into account. Stationary deconvolution only treats the frequency domain problems associated with attenuation, such as broadening of the seismic pulse, and spectral decay. The time domain problems, such as amplitude decay, must be corrected for with a gain operator. The undesirable effects in the time and frequency domains were created through the same process and a method that compensates for them both simultaneously would be advantageous.

Inverse-Q filters are deterministic nonstationary filters that attempt to remove the effects of anelastic attenuation. In general, inverse-Q filters explicitly model the anelastic attenuation and attempt to correct seismic data for the amplitude and phase effects. Unfortunately, such methods generally have a high reliance on an estimate of Q, which is notoriously difficult to estimate. In addition, a deconvolution must be applied separately to remove the effects of source signature. Inverse-Q filters have several advantages and weaknesses. If the constant-Q model applies, inverse-Q filters remove absorption and increase the stationarity and resolution of a seismic section. The inverse-Q filters are, in general, deterministic and tend to apply a theoretical model to a seismic section therefore their weaknesses include a high reliance on the parameter Q.

NSD approximately corrects for anelastic attenuation, phase distortion and source signature. The purpose of NSD is to correct for time and frequency-domain effects simultaneously, in accordance with our understanding of how earth processes created these effects in the data. NSD has been developed from a model of a wavelet propagating through a 1-D earth that suffers frequency-dependent attenuation and dispersion along its travelpath. NSD estimates and removes them in a time and frequency dependent manner. The NSD operator also estimates and removes source signature. In a lossless medium (Q approaches infinity) the propagating wavelet is time-invariant and the NSD process becomes stationary frequency-domain deconvolution and only removes the source signature. NSD can be considered as a type data-driven inverse-Q filter with additional capability to remove the source signature.

METHOD

Nonstationary spectral model

The purpose of NSD is to recover the reflectivity from a seismic trace by removing the source signature and nonstationary propagation effects. To achieve this, a model that relates the $|TVS|$ of the input trace to those effects which should be removed is required. In this section, the nonstationary convolutional model of the input trace will be developed from the stationary convolutional model.

The spectrum of a seismic trace, $S(f)$ can be modelled by the stationary convolutional model in the frequency domain as

$$S(f) = R(f)M(f)W(f) \quad (1)$$

where $R(f)$ is the spectrum of the reflectivity, $M(f)$ is the spectrum of the multiples and $W(f)$ is the source signature. An extension of the stationary convolutional model, Equation (1), into the nonstationary realm is postulated. The nonstationary (dependent on time and frequency) spectrum, $S(t,f)$, of a raw 1-D seismic trace can be modeled as

$$S(t,f) = R(t,f)M(t,f)W(f)e^{-\pi a(t,f)ft + i\phi(t,f)}, \quad (2)$$

where $R(t,f)$ is the TVS of the earth's reflectivity function, $M(t,f)$ is the nonstationary spectrum describing multiple reflections, $W(f)$ is the stationary spectrum of the source signature including stationary near surface effects, $a(t,f)$ is a generalized attenuation function, and $\phi(t,f)$ is the minimum-phase spectrum associated with attenuation (Futterman, 1962). If $a=1/Q(t)$, the exponential attenuation becomes the constant Q model of attenuation (Kjartansson, 1979). Note that if the time dependence of Equation (2) vanishes, then the stationary convolutional model, Equation (1), results. Thus the nonstationary convolutional model can be considered 'locally' stationary. The magnitude of Equation (2) can be taken to obtain a relationship between the amplitudes of each component:

$$|S(t,f)| = |R(t,f)| |M(t,f)| |W(f)| e^{-\pi a(t,f)ft}. \quad (3)$$

The $|TVS|$ of the physical forward operator can be inferred from Equation (3). The physical forward operator is called the propagating wavelet and it acts on the reflectivity. Its nonstationary amplitude spectrum, $|W_p(t,f)|$, can be modeled as

$$|W_p(t,f)| = |M(t,f)| |W(f)| e^{-\pi a(t,f)ft}. \quad (4)$$

$|W_p(t,f)|$ gives the Fourier amplitude spectrum of the propagating wavelet for a fixed time, t . The propagating wavelet contains the attenuation and source effects and it physically represents a wavelet propagating through a 1-D earth, attenuating with time, and accumulating a multiple train.

Time-variant spectrum

A TVS is basically a decomposition of a time series onto a time-frequency matrix. Each spectrum, localized at a particular time, $TVS(\tau,f)$, is calculated by taking the *short-time Fourier transform* (Cohen, 1995),

$$TVS(\tau,f) = \int x(t)h(t-\tau)e^{-i2\pi ft} dt, \quad (5)$$

where $x(t)$ is the trace and $h(t-\tau)$ is a time-shifted window. A window is a function whose magnitude is localized near the origin and decays rapidly elsewhere. It is designed to suppress the signal at distant times and leave it unaltered around the time,

$t=\tau$. When multiplied with a signal a window serves to localize the properties of that signal in time.

The time-variant amplitude spectrum, $|\text{TVS}|(\tau,f)$, can be calculated by taking the magnitude of Equation (5). The amplitude spectrum, $|\text{TVS}|(\tau,f)$, becomes a row in the time-frequency grid at time, τ , and it measures the frequency distribution localized around that time. The window is incremented along the trace, with an overlap of typically 70-90% between windows, and the $|\text{TVS}|(\tau,f)$ is calculated for each window increment. Each amplitude spectrum will form a row in the resulting grid. Figure 1 depicts how the $|\text{TVS}|$ is calculated. In the grey level $|\text{TVS}|$ display, black represents large positive numbers and white is zero.

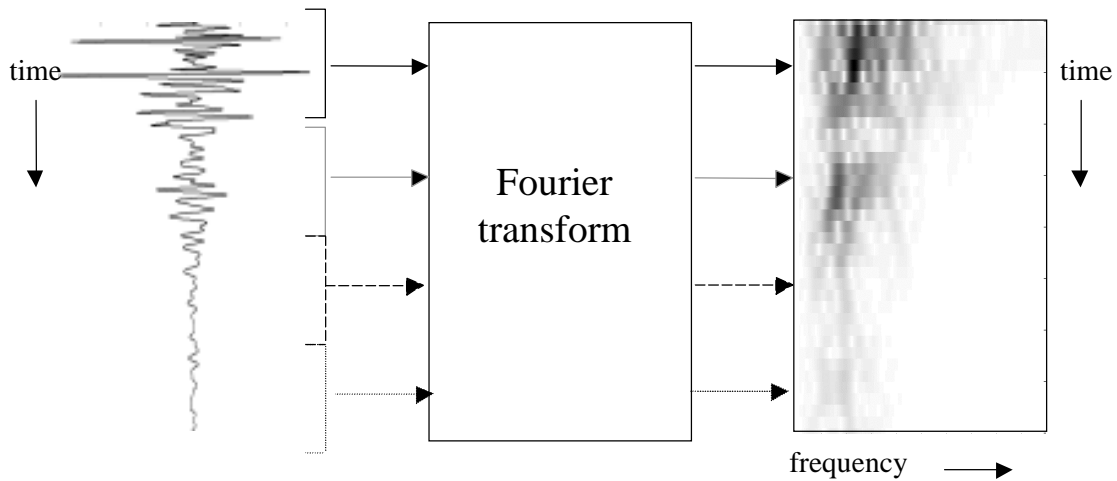


Figure 1: Calculation of a $|\text{TVS}|$ from an input trace. The trace is windowed and the Fourier transform of each windowed segment is calculated. The resulting amplitude spectrum forms a row in the resulting $|\text{TVS}|$ grid. In the grey level $|\text{TVS}|$ display, black represents large positive numbers and white is zero.

The trace in Figure 1 is a synthetic trace created by applying a Q filter ($Q=25$) superimposed with a minimum-phase wavelet, to a reflectivity series. The $|\text{TVS}|$ is therefore composed of the time-variant spectra of the source signature, reflectivity and attenuation. The source waveform is stationary and bandlimited. It is the broad spectrum at early times and is marked by the absence of very low frequencies as can be seen from Figure 1. From Figure 1, it can also be seen that this initial spectrum decays rapidly in both time and frequency. This exponential attenuation dominates the $|\text{TVS}|$ and the effects of reflectivity provide detail in the $|\text{TVS}|$.

The window increment is an important parameter in the $|\text{TVS}|$ computation because it is essentially the time sample interval of the $|\text{TVS}|$. In addition, the window increment is inversely proportional to the computation time of the $|\text{TVS}|$. Therefore this parameter must be chosen carefully so that the computation time of the $|\text{TVS}|$ is reasonable and the time-variant effects which are to be examined are faithfully recorded in the $|\text{TVS}|$. This is a concern for NSD as the steep exponential

attenuation inherent in an anelastically attenuated input trace may be distorted or aliased if the trace is sampled too coarsely.

Another important parameter in the calculation of the $|TVS|$ is the window length. The resolution of the $|TVS|$ in time and frequency is determined by window length as governed by the uncertainty principle (Cohen, 1995). The uncertainty principle is given by

$$TB \geq \text{constant} \quad (6)$$

where T is the duration of a signal and B is the bandwidth of its spectrum. The duration of the signal is determined from the length of the window that has been applied to the seismic trace. A detailed proof of the uncertainty principle can be found in Cohen (1995). In a few words, the uncertainty principle is the property that a narrow time-domain signal will have a broad bandwidth and a broad time-domain signal will have a narrow bandwidth. The bandwidth and duration of a signal cannot both be made arbitrarily narrow simultaneously.

The choice of window length has important implications regarding the time and frequency resolution of the $|TVS|$. A $|TVS|$ created with a long window will have excellent resolution in frequency but poor temporal resolution, and a $|TVS|$ created with a short window will have greater time resolution at the expense of frequency resolution. The $|TVS|$ cannot have ideal time and frequency localization simultaneously. Therefore a decision must be made about the purpose of the $|TVS|$ and whether time or frequency resolution has priority, when choosing a window length.

Operator design and application

A nonstationary operator, designed directly from the input data, containing the source signature as well as undesirable characteristics related to anelastic attenuation is desired. This operator will be called the forward operator. It is assumed that the reflectivity effects can be removed from the nonstationary power spectrum ($|TVS|^2$) of the input trace through smoothing and that the smoothed $|TVS|$ will be an estimate of the forward operator.

Two methods of smoothing, simple and residual, have been developed for NSD. However, only one method, residual-smoothing, will be described in this paper. Both types of smoothing are more completely described in Schoepp (1998). The residual-smoothing method removes an approximate attenuation/gain surface from the $|TVS|$ of the gained input trace, squares the result and smoothes the resulting residual power spectrum. The approximate attenuation/gain surface is restored to the square root of the residual power spectrum (the amplitude spectrum) after smoothing. As with stationary deconvolution techniques, smoothing methods will imperfectly remove reflectivity effects and bias the amplitude spectrum of the embedded wavelet. It is unclear what the smoothing does to $|M(t,f)|$.

After smoothing, the forward operator can be left as zero phase or coupled with a minimum-phase spectrum, which seems reasonable as the earth is expected to

have minimum-phase attenuative processes. The forward operator is then inverted and applied to the data using nonstationary filter theory (Margrave, 1998).

Gain of input trace and calculation of the |TVS|

The first step of the NSD algorithm is to apply an approximate and deterministic exponential gain to the input trace. This is done to reduce aliasing of the steep decay surface of the input trace when it is windowed during the calculation of the |TVS|. Exponential gain of the input trace is a computational convenience and allows the |TVS| to be sparsely sampled in time.

After gain has been applied to the input trace, its |TVS| is calculated. This |TVS| will be processed to form the NSD operator. A model for the |TVS| of the gained input trace, $|S(t,f)|$, follows from Equation (6) (assuming constant-Q attenuation) as

$$|S(t,f)| = |R(t,f)| |M(t,f)| |W(f)| e^{-\pi ft/Q + \lambda t}, \quad (7)$$

where λ is an exponential gain constant. The nonstationary power spectrum of the gained input trace, $|S(t,f)|^2$, is calculated by squaring Equation (7)

$$|S(t,f)|^2 = |R(t,f)|^2 |M(t,f)|^2 |W(f)|^2 e^{-2\pi ft/Q + 2\lambda t}. \quad (8)$$

Smoothing

The next step in the NSD process is to attempt to separate the reflectivity from the source waveform and attenuation. Two methods of smoothing have been developed for NSD, however only one method, the residual-smoothing method, will be outlined in this paper. In the residual-smoothing method, the steep Q/gain surface is removed from the |TVS| of the gained input trace before smoothing to reduce the bias of the operator. An estimate of Q is required in this removal process.

Constant-Q attenuation can be modeled as an exponential surface in frequency and time whose shape is determined by the quality factor, Q (assumed to be constant in frequency and slowly time-variant). Assuming that an estimate of Q, \hat{Q} , is available, and setting $|M(t,f)|$ to unity (to ignore multiple effects), the attenuation/gain surface can be removed approximately from $|S(t,f)|$ of Equation (8) to produce a residual amplitude spectrum, $|\rho(t,f)|$,

$$|\rho(t,f)| = \frac{|R(t,f)| |W(f)| e^{-\pi ft/Q + \lambda t}}{e^{-\pi ft/\hat{Q} + \lambda t} + n_Q}, \quad (9)$$

where n_Q is the maximum of the exponential decay/gain surface multiplied by a small constant. The constant, n_Q , is added to increase stability in the division caused by finite numerical precision. The constant is typically small, between 1×10^{-4} and 1×10^{-6} .

Equation (9) can be written approximately as

$$|\rho(t,f)| \approx |R(t,f)| |W(f)|. \quad (10)$$

The residual amplitude spectrum, $|\rho(t,f)|$, is mostly free from attenuation effects and is dominated by the amplitude spectra of the source signature and reflectivity. This residual amplitude spectrum is squared to form a power spectrum and then smoothed two-dimensionally with time and frequency smoothers to remove the reflectivity and estimate $|W(f)|$.

$$\overline{|\rho(t,f)|^2} \approx |R(t,f)|^2 |W(f)|^2 *a(f) *b(t), \quad (11)$$

where $\overline{|\rho(t,f)|^2}$ is the residual power spectrum after smoothing, $*$ denotes convolution, $a(f)$ is the frequency smoother and $b(t)$ is the time smoother. The smoothers may be different from the smoothers in the simple-smoothing method.

By removing the Q/gain surface, the reflectivity effects can be suppressed in the $|TVS|$ while reducing the bias from smoothing. Therefore, by assumption, the amplitude spectrum of the smoothed residual can be written as

$$\overline{|\rho(t,f)|} \approx |W(f)|. \quad (12)$$

From Equation (12) it can be seen that $\overline{|\rho(t,f)|}$ is an estimate of the stationary source amplitude spectrum.

After the residual-smoothing process, the attenuation/gain surface is restored to $\overline{|\rho(t,f)|}$. This yields an estimate of the amplitude spectrum of the gained forward operator, $|F(t,f)|$:

$$|F(t,f)| \approx \overline{|\rho(t,f)|} e^{-\pi ft/Q+\lambda t} + n_w, \quad (13)$$

where n_w is a constant added for stability in the inversion of Equation (17). The constant, n_w , is determined by multiplying the maximum of $|\rho(t,f)| e^{-\pi ft/Q+\lambda t}$ by a small number, typically between 10^{-1} and 10^{-6} . The quantity, $|\rho(t,f)| e^{-\pi ft/Q+\lambda t}$, will contain noise if it has been calculated from real data. The constant is added to prevent noise in areas of low signal strength from dominating $|F(t,f)|$ after the inversion.

The physical forward operator is called the propagating wavelet and it contains the source waveform and attenuation effects,

$$|W_p(t,f)| \approx \overline{|\rho(t,f)|} e^{-\pi ft/Q}. \quad (14)$$

The propagating wavelet differs from the forward operator in that it does not have exponential gain.

Phase computation, inversion, and application of the operator

The operator may be left as zero phase or combined with a minimum-phase spectrum. Although each row of the 'zero-phase' operator is zero phase, such operators will generally change both the amplitude and the phase of a trace when applied using nonstationary filter theory (Margrave, 1998). The minimum-phase spectrum is calculated with a one-dimensional Hilbert transform, H , over frequency at constant time of the natural logarithm of the amplitude spectrum:

$$\phi(t,f) = H[\ln |F(t,f)|], \quad (15)$$

From Equation (13) it can be seen that the forward operator contains a small constant to prevent the logarithm in Equation (15) from becoming unstable. The operation of Equation (15) is performed on each row of the time-variant amplitude spectrum to create a time-variant minimum-phase spectrum. The amplitude spectrum, $|F(t,f)|$ of Equation (11) and the phase spectrum, $\phi(t,f)$, of Equation (15) can be combined to produce the complex-valued forward operator, $F(t,f)$

$$F(t,f) = |F(t,f)| e^{i\phi(t,f)}. \quad (16)$$

To complete the process, the forward operator, $F(t,f)$, is inverted and applied to the trace using nonstationary filter theory (Margrave, 1998). In this manner, the time-variant operator is applied continuously to the input trace and windowing is avoided in the operator application. The spectrum of the reflectivity estimate, $R(f)$, is given by

$$R(f) = \int s(t) F^{-1}(t,f) e^{-2\pi i t f} dt, \quad (17)$$

where $s(t)$ is the input trace and $F^{-1}(t,f)$ is the inverse operator that is the simple algebraic inverse of $F(t,f)$. The forward and inverse operators are related for all t and f by

$$F(t,f) F^{-1}(t,f) = 1 \quad (18)$$

An inverse Fourier transform is applied to $R(f)$ to obtain the reflectivity estimate in the time domain.

The success of the inversion in NSD is partly limited by numerical precision. Finite numerical precision causes amplitude distortion of the most severely attenuated frequencies. These amplitude distortions are magnified by inversion and are manifested as noise in the final result from NSD. The bandwidth of $R(f)$ must be limited by applying a bandpass filter after NSD to suppress frequencies affected by this lack of numerical precision. The bandpass filter should be chosen to encompass frequencies that may be contained in the spectrum of the source waveform and suppress all frequencies greater than Nyquist frequency. Noise may dominate the signal where it is severely attenuated, such as at high frequencies. This noise may be magnified during the phase computation or operator inversion, if insufficient amounts of white noise, n_w , have been added.

Profile-mode NSD

NSD, as described above, designs and applies an operator separately for each trace. This original trace-by-trace version of NSD has been modified in an effort to improve efficiency and allow more flexibility. The modified version of trace-by-trace NSD, profile-mode NSD, designs a single operator and applies it to an entire ensemble of traces. This option is designed to minimize trace to trace changes induced by the operator. In addition, a physical model of the data may indicate that a single operator is more appropriate for an entire ensemble. For example, a surface-consistent approach may require that a single operator be applied to an entire CMP gather.

The operator in profile-mode NSD is created by calculating a $|TVS|$ for each trace in the ensemble and averaging them to produce a single $|TVS|$. This resulting $|TVS|$ is processed as the $|TVS|$ of any input trace is processed in trace-by-trace NSD. Specifically, the average $|TVS|$ is smoothed, coupled with a minimum-phase spectrum if desired, and inverted to form the NSD operator. However in the profile-mode approach, the single NSD operator (created from the average $|TVS|$) is applied to each trace in the ensemble. Profile-mode deconvolution is a great advantage in that it provides greater trace-to-trace stability.

EXAMPLES

NSD has been applied to the Blackfoot broadband survey to test performance on real data. The Blackfoot broadband 2D survey was acquired in 1995 over the Blackfoot Field near Strathmore, Alberta. The target in this area is glauconitic channel sands, up to 35m in thickness, deposited in the Lower Cretaceous as incised valley fill (Stewart et al., 1996). The channel sands overlie carbonates of Missippian age. The processing goal is to delineate the channel boundaries and image the target.

The data was processed several times to allow for different comparisons. A dataset deconvolved with gain and Wiener deconvolution will be compared to a dataset deconvolved with Wiener deconvolution and inverse-Q filtering, and a dataset deconvolved with NSD. The comparisons of the deconvolved data will involve:

1. entire stacked datasets
2. average $|TVS|$ of datasets
3. comparison of the area thought to contain the channel
4. comparison of deconvolved traces to the synthetic seismograms

Processing the Blackfoot Broadband survey

All examples in this paper have been created with basically the same processing flow. Variations have been made to this basic flow only to accommodate different deconvolutions: Flow 1 is the NSD flow, Flow 2 is the gain and Wiener deconvolution flow and Flow 3 includes Wiener deconvolution and inverse-Q filtering.

An estimate of Q is required for NSD and inverse-Q filtering. This estimate was calculated to be 100 with the spectral ratio method (White, 1992). This Q value seems consistent with the lithology of the region (sands, shales, dolomites and limestones).

NSD was applied post-stack for computational ease. The surface consistent model (Levin, 1989) suggests that constant-Q attenuation is expected to be midpoint consistent and therefore applying NSD to data stacked by common midpoint is acceptable. Wiener deconvolution and the inverse-Q filter were also applied post-stack to provide a fair comparison with NSD.

Below is a description of the processing flow. Each processing technique was applied to every dataset unless specified otherwise.

1. *mute*
2. *spherical divergence corrections*
3. *gain* (Flows 1 and 2) A gain correction of 6dB/s was applied to the Wiener deconvolution dataset and the NSD dataset. The gain will be removed from the NSD dataset during the NSD process. Gain was not applied to the dataset that was inverse-Q filtered.
4. *elevation statics*
5. *residual statics*
6. *bandpass filter* A zero-phase Ormsby bandpass filter of 8-12-90-120 Hz was applied to the datasets.
7. *normal moveout (NMO) correction*
8. *stack*
9. *NSD* (Flow 1) The minimum-phase residual-smoothing version of profile-mode NSD with a 1.0s time smoother and a 10 Hz frequency smoother was applied. A stabilization factor of 0.01 was used in the algorithm. A time-variant filter with a high cut of 160 Hz at 0s and 70 Hz at 2s was applied to the NSD datasets. A Q value of 100 was used in the NSD algorithm.
10. *Wiener deconvolution* (Flows 2 and 3). A minimum-phase Wiener deconvolution was applied to one of the datasets. An operator of 100ms in length and 0.01 stabilization factor was used. The operator was designed on the time zone of 500-1500ms. These parameters were chosen to be consistent with NSD.
11. *inverse-Q filtering* (Flow 3) Inverse-Q filtering was applied to only one dataset. A Q value of 100 was used for all traces at all times.
12. *trace equalization*

13. *FX spatial prediction* A Wiener-Levinson algorithm was used with 0% white noise, a spatial operator of 60 traces, and 5 samples in the prediction filter. The windows are 300ms in length with a 30ms overlap. Frequencies below 5Hz and above 160Hz were attenuated.

14. *phase shift migration* The data was migrated from CDP 260 to CDP 550 to avoid end effects. Frequencies of 0 to 160 Hz were migrated.

15. *automatic gain control* (Flow 2)

Comparison of NSD to other deconvolution techniques

Two wells near the Blackfoot broadband survey containing sonic and density logs, 14-09-023-23W4 and 4-16-023-23W4, allow for the construction of synthetic seismograms. Figure 2 is a map showing the location of the two wells in relation to the line. The two wells are pointed out in Figure 2 by arrows.

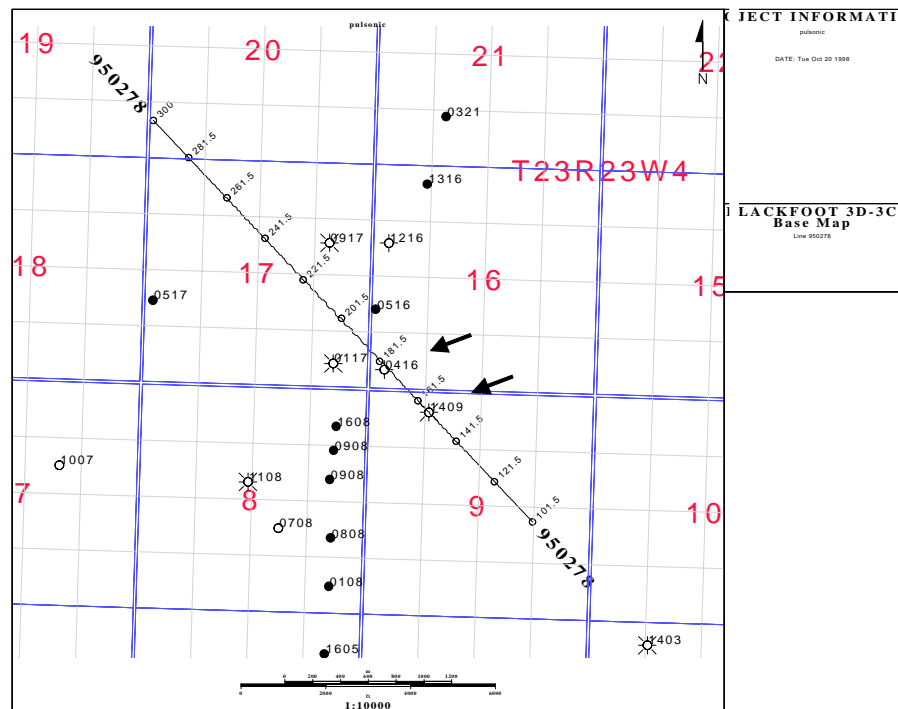


Figure 2: A map showing the location of 14-09 and 4-16 in relation to the Blackfoot broadband survey. Arrows in the figure point out the two wells.

Synthetic seismograms in these examples are one-dimensional and do not contain multiple effects. The layers are assumed to be horizontal and the raypaths are assumed to be vertical (and therefore normally incident on the reflectors). In addition, diffractions and other wave modes are ignored. The wavelet used in the model is an Ormsby wavelet with corner frequencies of 8-12-90-110 Hz for the 4-16 synthetic and an Ormsby wavelet with corner frequencies of 8-12-75-90 for the 14-09 synthetic seismogram. The 4-16 sonic log has been check-shot corrected to reduce the time delay between synthetic seismograms and seismic data.

In this section, the results from NSD will be compared to results from a combination of gain and Wiener deconvolution, and Wiener deconvolution and inverse-Q filtering. Figure 3 shows the stacked data set after pre-stack processing without application of any deconvolution. The stack with gain and Wiener deconvolution applied to it is shown in Figure 4. The stack with Wiener deconvolution and inverse-Q filtering is shown in Figure 5, and the stack with NSD is shown in Figure 6. Figure 7 shows an average |TVS| for each stacked section. The average |TVS| were calculated by averaging the |TVS| of traces 50 to 100. A zoom of the area thought to contain the channel of each of the three stacks is shown in Figure 8 and a comparison of the datasets to the synthetic seismograms is shown in Figures 9 and 10.

All deconvolved sections show increased resolution as compared to the stack before post-stack processing (Figure 3). The stacked section with post-stack NSD deconvolution seems to be of better resolution than the other two sections, although comparison is difficult at this scale. The reflectors in the 1300 to 1600 ms time zone seem to be more resolved on the NSD section.

The average |TVS| are shown in Figure 7. In these grey level plots, white is zero and black is a large positive number. The average |TVS| of the sections processed with gain and Wiener deconvolution, and Wiener deconvolution and inverse-Q filtering are dominated by two separate high amplitude areas. In addition, both average |TVS| are lacking high frequencies at later times. In contrast, the average |TVS| of the NSD result is more even and consistent. The bandwidth is approximately 10 to 110 Hz.

As stated previously, the target in this area is channel sands. Figure 8 focuses in on the area of each of the deconvolved sections thought to contain the target. The geological feature thought to be the channel is pointed out with arrows. The channel is difficult to discern on the section deconvolved with post-stack Wiener deconvolution and on the section that had Wiener deconvolution and inverse-Q filter applied to it. The section with NSD shows the best image of the target. The channel in the NSD section is outlined by the underlying Mississippian carbonates. In addition there is an internal marker in the channel sands at approximately 1060ms in the NSD section that stands out clearly. This internal marker is absent in the other sections. The vertical resolution of the NSD result seems improved as compared to the others.

The comparisons of the different processing flows with the 14-09 synthetic seismogram are shown in Figure 9. The 14-09 synthetic seismogram ties reasonably well to the seismic sections. The NSD section ties better to the synthetic seismogram at later times, such as 0.7s to 0.8s, than the other seismic sections.

The 4-16 synthetic seismogram ties more closely to the Blackfoot broadband survey, as can be seen from Figure 10. Again, the NSD result matches the synthetic better than the other two sections. The trough at 0.92s (shown by an arrow in the figure) on the synthetic seismogram of 4-16 is best approximated by the NSD result. The time zone between 0.97s and 1.01s (also pointed out by an arrow) is also best matched by the NSD result.

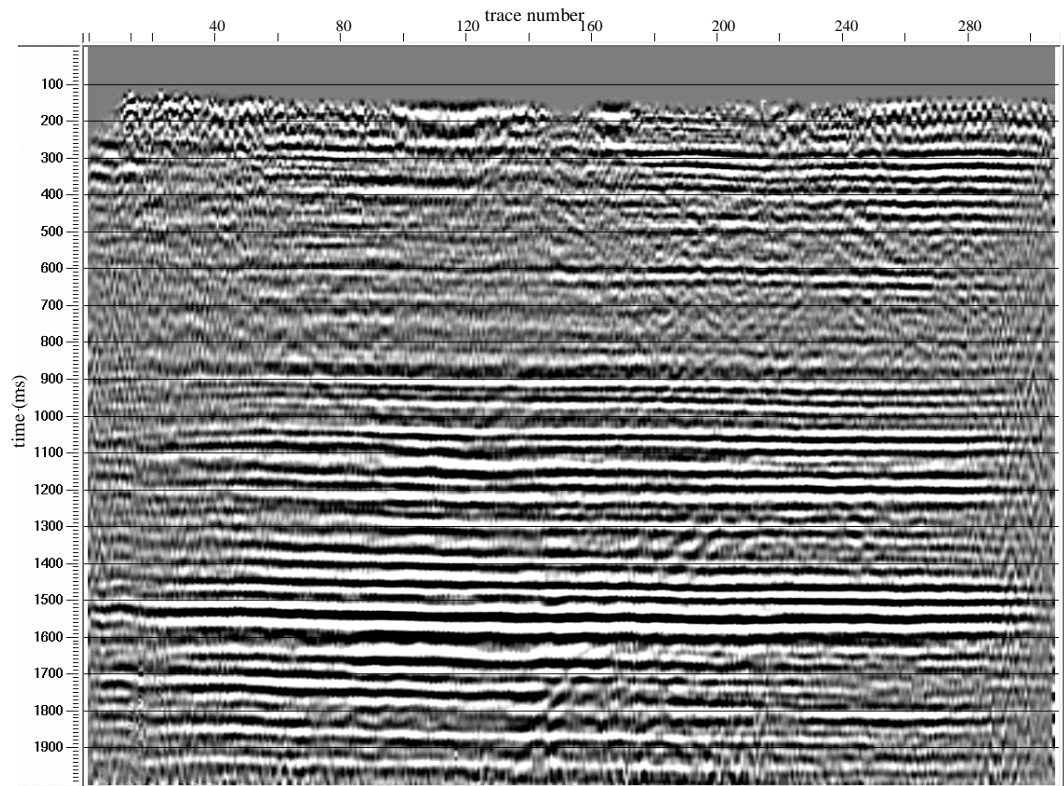


Figure 3: The Blackfoot broadband survey after pre-stack processing and without application of any deconvolution.

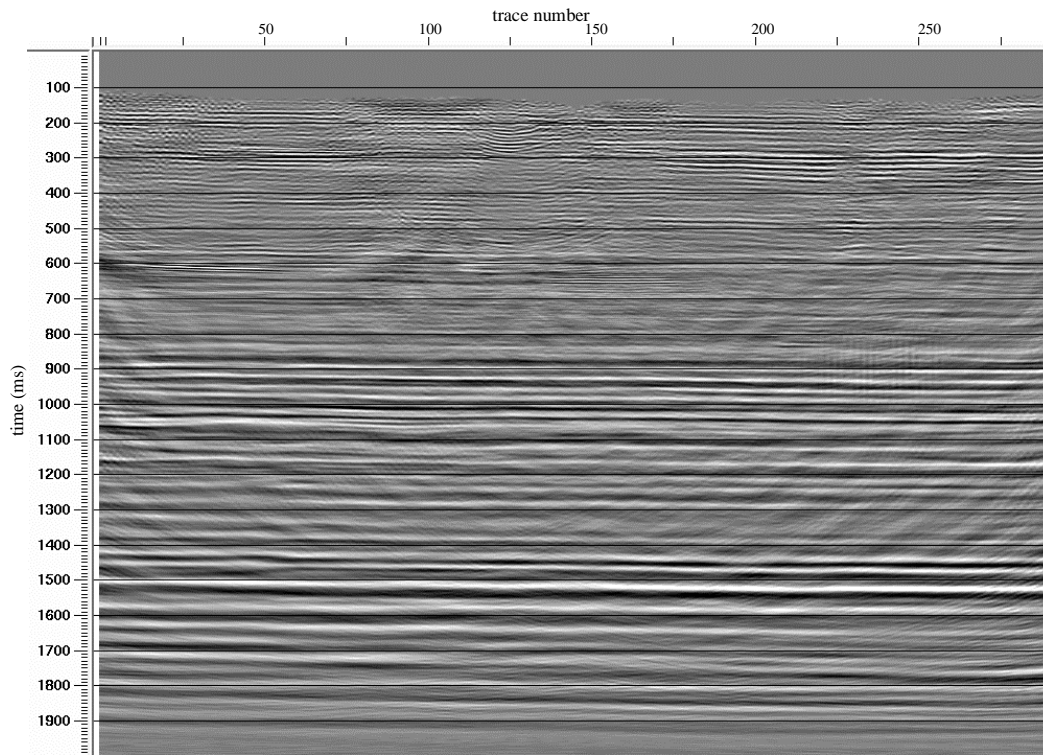


Figure 4: The Blackfoot broadband survey with gain and post-stack Wiener deconvolution and the complete post-stack flow described in the text.

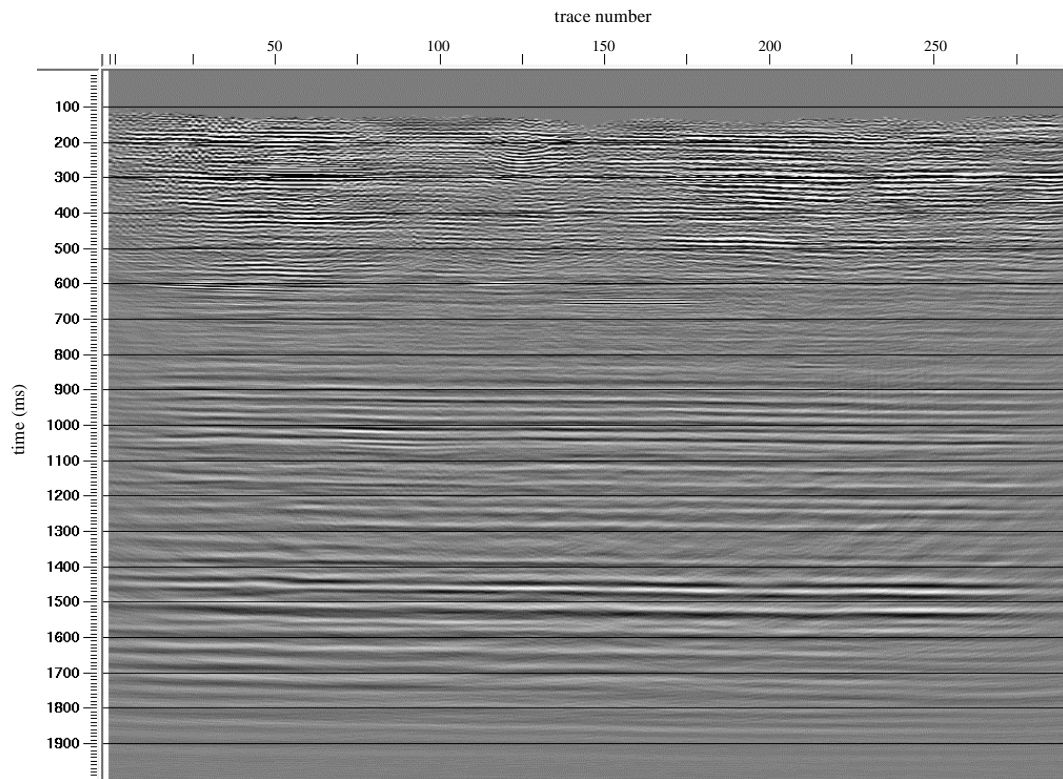


Figure 5: The Blackfoot broadband survey with post-stack Wiener deconvolution and post-stack inverse-Q filtering and the complete post-stack flow described in the text.

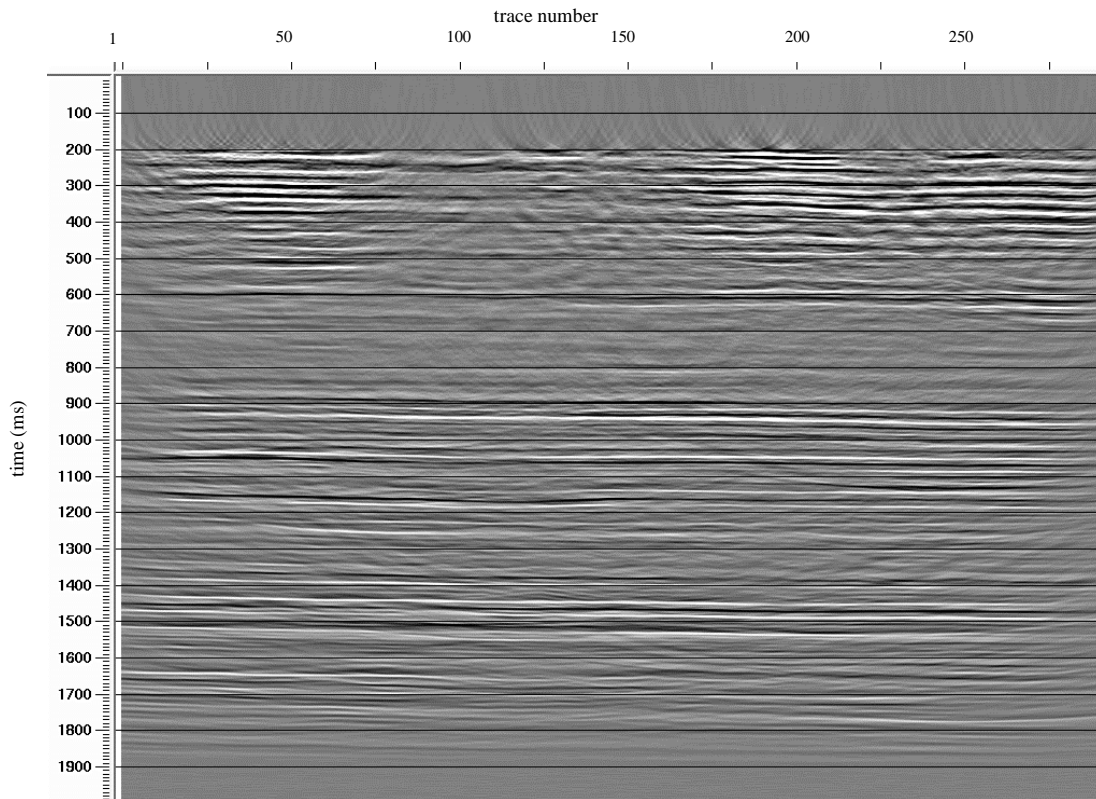


Figure 6: The Blackfoot broadband survey with post-stack NSD and the complete post-stack flow described in the text.

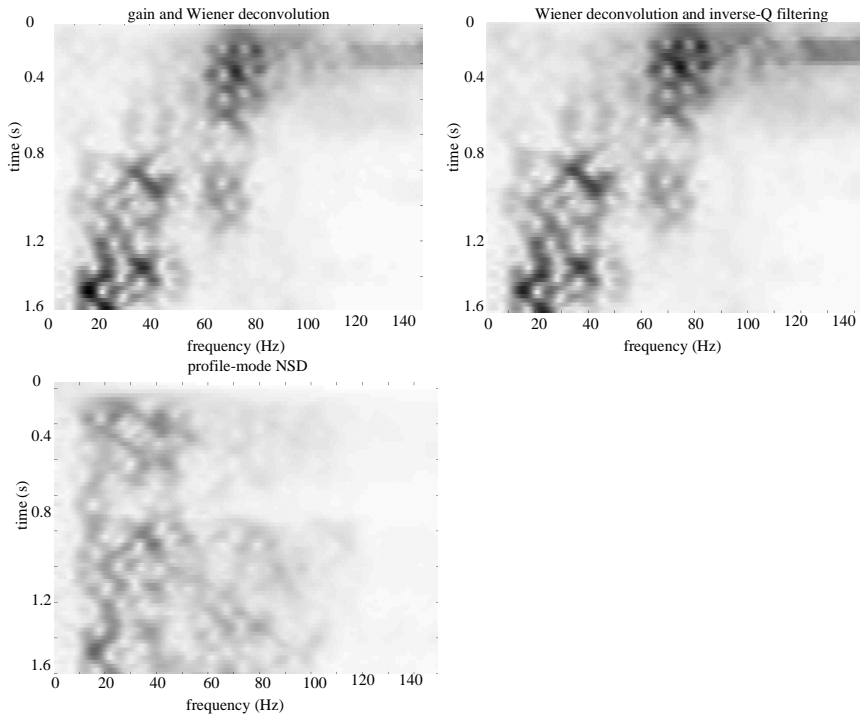


Figure 7: The average |TVS|, calculated by averaging the |TVS| of traces 50 to 100, of the stacked sections from Figures 4 to 6.

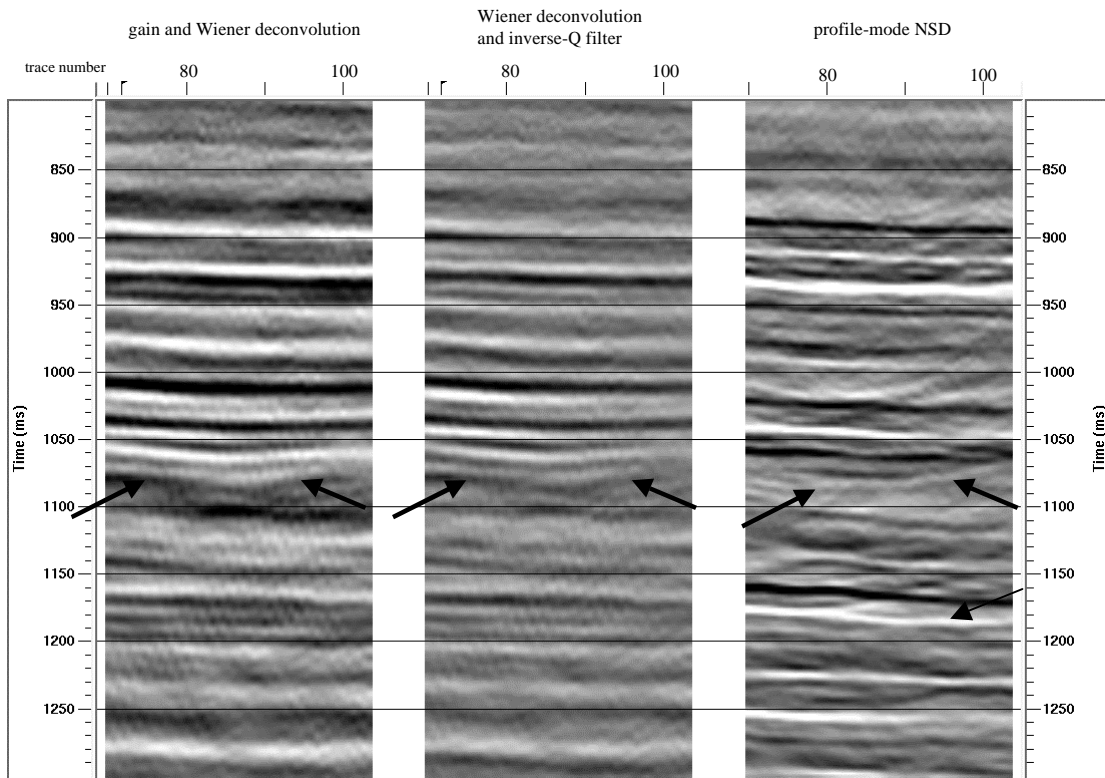


Figure 8: The target area of each of the deconvolved sections. The feature thought to be the channel is pointed out with arrows in the figure.

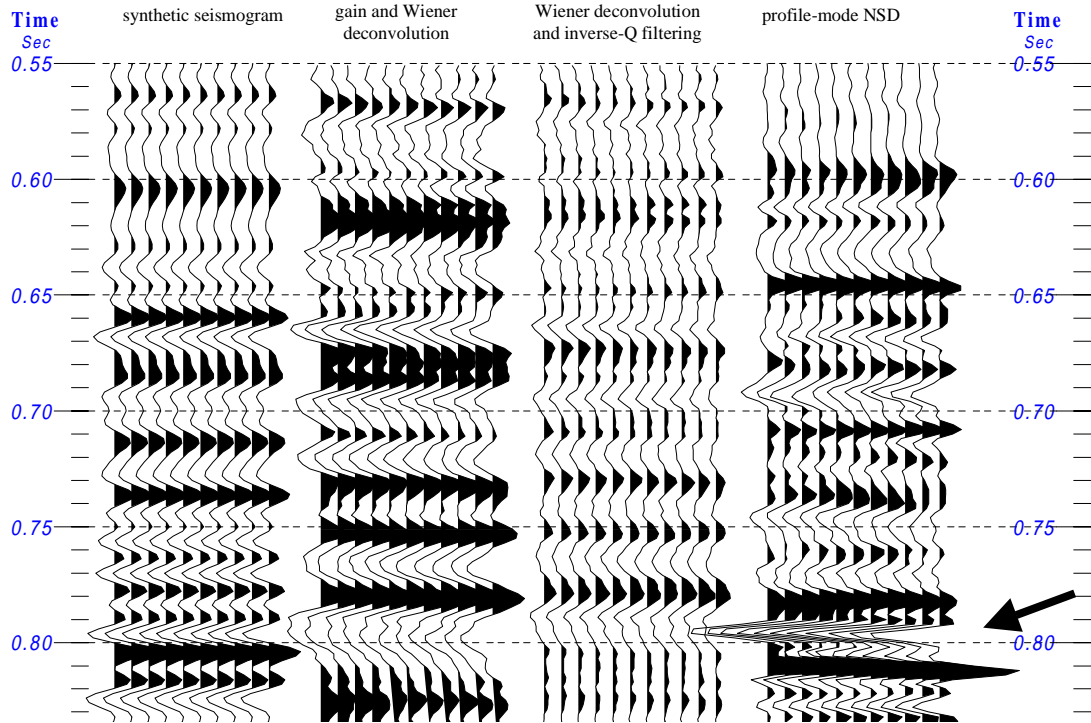


Figure 9: The 14-09 synthetic seismogram compared to the result from gain and post-stack Wiener deconvolution, post-stack Wiener deconvolution and post-stack inverse-Q filtering and post-stack NSD.

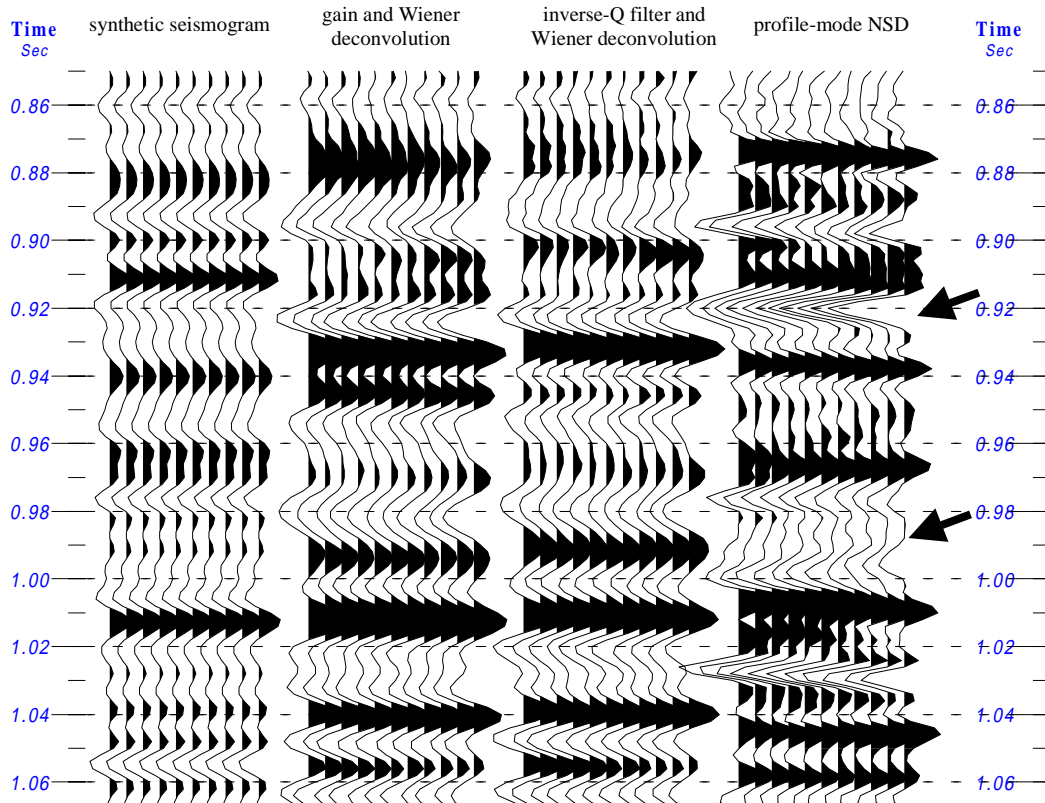


Figure 10: The 4-16 synthetic seismogram compared to the result from gain and post-stack Wiener deconvolution, post-stack Wiener deconvolution and post-stack inverse-Q filtering and post-stack NSD. The arrows point to places on the synthetic seismogram that tie best with the NSD result.

Comparison of extensions of NSD

A comparison was made of trace-by-trace NSD and profile-mode NSD using the Blackfoot broadband survey. Again, NSD was applied post-stack for computational ease and the parameters used for NSD were the same as the previous examples. The full seismic sections of the Blackfoot Broadband survey processed with both versions of NSD are not shown, as they were indistinguishable from each other at the scale shown in this paper. The result from profile-mode NSD is shown in Figure 6. The average $|TVS|$, created by averaging the $|TVS|$ of traces 50 to 100, of both sections deconvolved with NSD, are shown in Figure 11. Figure 12 is a comparison of a zoom of both sections in the area where the channel is thought to be.

The average $|TVS|$ and the zoom of the channel look very similar for both versions of NSD. Slight differences however can be seen in the zoomed section of the comparison to synthetic seismograms in Figures 13 and 14. The reflectors in the trace-by-trace NSD result appear less consistent. For example the peak at 0.62s on Figure 13, as pointed out with an arrow, is more consistent in the profile-mode NSD. This is expected because applying a single operator to an ensemble of traces will reduce trace-to-trace differences. In general, the results from both types of NSD yield

similar results. The advantage of profile-mode NSD lies in statistical leverage and trace-to-trace stability.

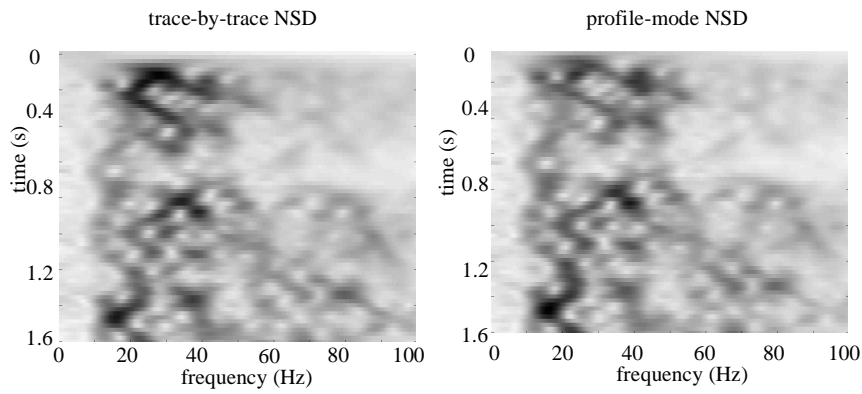


Figure 11: Average $|TVS|$ of trace-by-trace NSD and profile mode NSD. The average $|TVS|$ were calculated by averaging the $|TVS|$ of traces 50 to 100.

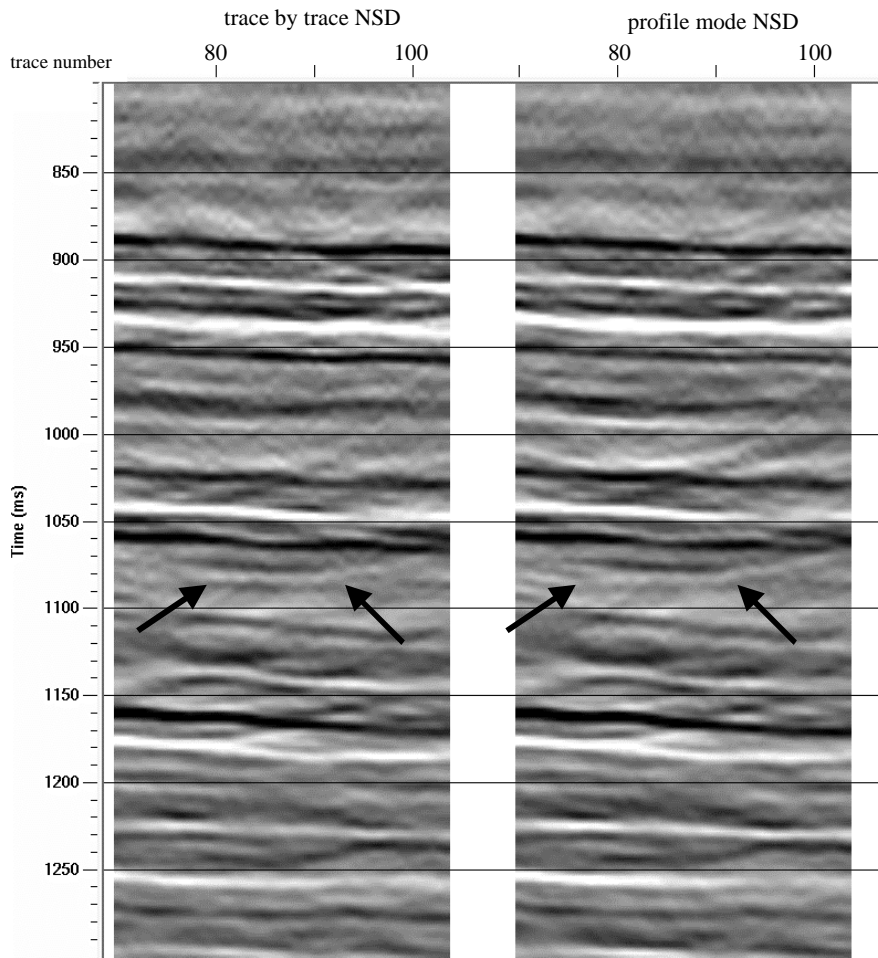


Figure 12: A comparison of profile-mode NSD and trace-by-trace NSD in the channel zone. The feature thought to be the channel is pointed out with arrows.

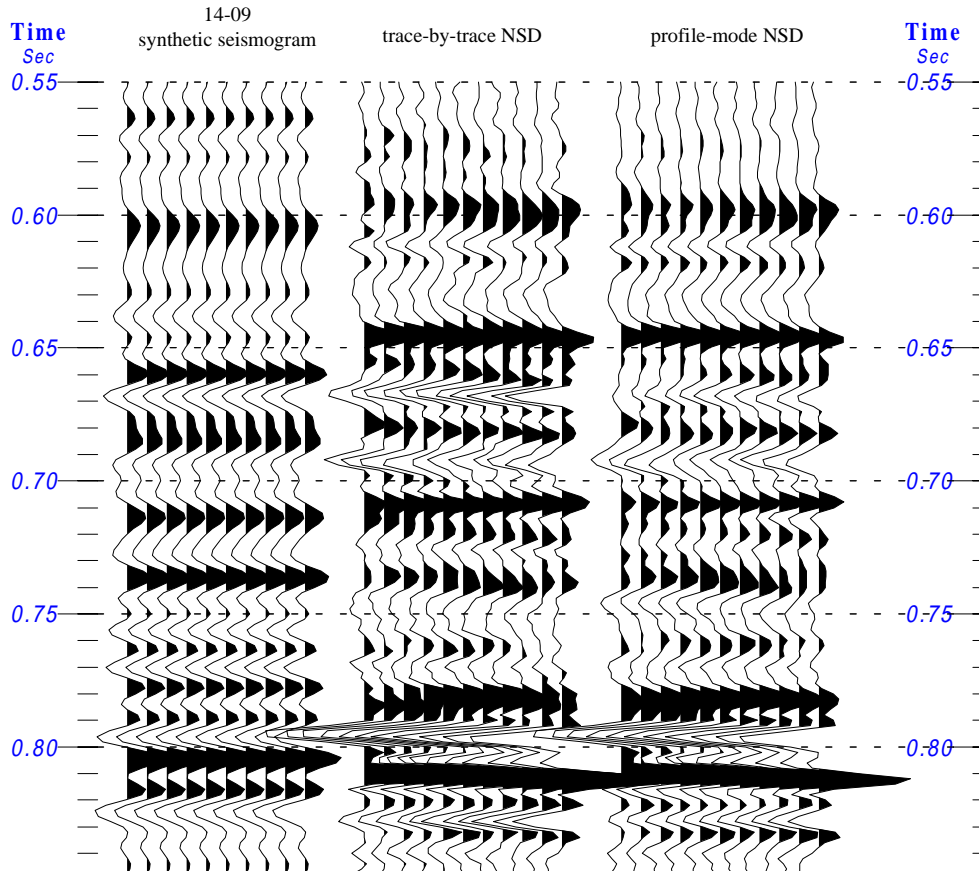


Figure 13: The 14-09 synthetic compared to trace-by-trace NSD and profile-mode NSD. Ten traces centered at the well for each NSD result are shown.

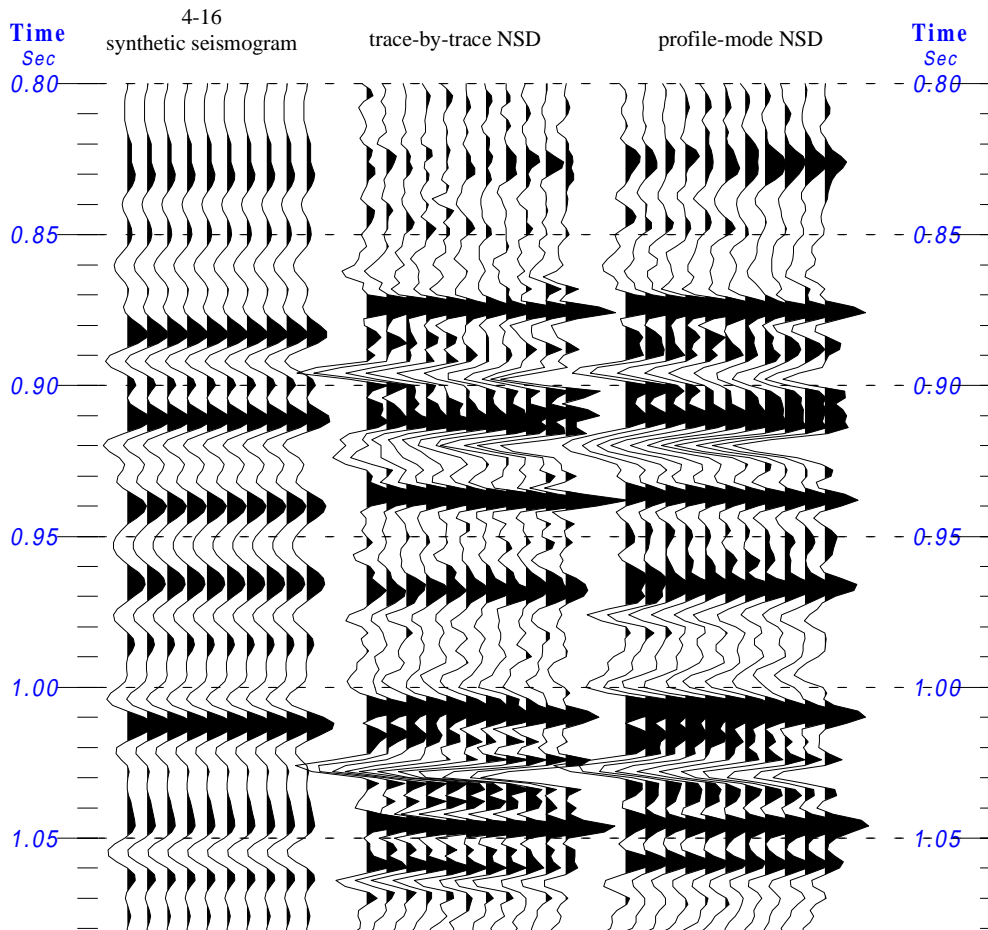


Figure 14: The 4-16 synthetic compared to trace-by-trace NSD and profile-mode NSD.

CONCLUSIONS

NSD has proved effective as applied to the Blackfoot broadband survey. It enhanced the vertical resolution of the stacked section as compared to the combinations of gain and Wiener deconvolution, and Wiener deconvolution and inverse-Q filtering. In addition, the section deconvolved with NSD has improved reflectivity character as compared to the other techniques. This is evident from the close-up view of the channel (Figure 8) and from the ties to the synthetic seismograms (Figures 9 and 10). In addition, the average $|TVS|$ of NSD is more even and consistent than the average $|TVS|$ of the other methods. NSD delineated the target channel more clearly than the other processing techniques. The success of NSD as compared to the other techniques is related to the physical model on which the operator is built and its data-driven nature.

NSD can be applied in two modes. In trace-by-trace mode an NSD operator can be designed and applied separately to each trace in an ensemble, and in profile mode a single operator can be designed from an ensemble and applied to each trace. The profile-mode NSD approach is useful when a physical model indicates that a single

operator is more appropriate. Profile-mode NSD reduces trace-to-trace differences induced by the operator and has a statistical advantage in the operator design.

ACKNOWLEDGEMENTS

We would like to thank the sponsors of the CREWES project for their support.

REFERENCES

- Cohen, L., 1995, Time-Frequency Analysis: Prentice Hall.
- Futterman, W. I., 1962, Dispersive body waves: Journal of Geophysical Research, **73**, 3917-393.
- Kjartansson, E., 1979, Constant Q wave propagation and attenuation: J. Geophys. Res., **84**, 4737-4748.
- Levin, S., 1989, Surface consistent deconvolution: Geophysics, **54**, 1123-1133.
- Margrave, G. F., 1998, Theory of nonstationary linear filtering in the Fourier domain with application to time variant filtering: Geophysics, **63**, 244-259.
- Schoepp, A. R., 1998, Improving seismic resolution with nonstationary deconvolution. MSc. thesis in progress.
- Stewart, R., Ferguson, R., Miller, S., Gallant, E., Margrave, G., F., 1996, The Blackfoot seismic experiments: broad-band, 3C-3D and 3D VSP surveys, CSEG Recorder (June, 1996).
- White, R. E., 1992, The accuracy of estimating Q from seismic data: Geophysics, **57**, 1508-1511.